Vibration mitigation using seismic metamaterials on layered soil

David Carneiro, Zohre Kabirian, Pieter Reumers, Geert Lombaert, and Geert Degrande

KU Leuven, Department of Civil Engineering, Structural Mechanics Section
Kasteelpark Arenberg 40 box 2448, B-3001 Leuven, Belgium

E-mail: david.carneiro@kuleuven.be

Abstract. This paper investigates how the soil profile affects the vibration mitigation performance of seismic metamaterials in a wide frequency band (1 – 80 Hz). A 3D coupled finite element - boundary element (FE-BE) model with an efficient substructuring method is developed to analyze the vibration reduction performance of seismic metamaterials on top of a layered soil. Resonators are modeled as single degree of freedom systems on top of square concrete surface foundations. The response of uniform and graded metasurfaces on a homogeneous and layered halfspace due to harmonic point load are compared. The narrow band gap obtained for a uniform metasurface on a homogeneous halfspace is widened over a broader range of frequencies (40 – 70 Hz) using inverse metawedges. For layered soil conditions, vibration mitigation in a wide frequency band still emerges using metawedges. Their efficiency, however, is reduced.

1. Introduction

Seismic metamaterials have been extensively studied as a mitigation measure of vibration in the built environment. These are artificially engineered materials consisting of an arrangement of elementary cells exhibiting non-conventional dispersion properties that are usually not found in natural soils [1]. Very promising results were reported to protect important civil infrastructure from earthquakes [2, 3].

Non-resonant seismic metamaterials induce Bragg scattering as result of periodic arrangements of the same order of the surface wavelengths, creating band gaps where wave propagation is not possible. Locally resonant seismic metamaterials on the other hand do not rely on structural periodicity, so that their dimensions and spacings can be lower than the surface wavelengths. These can be resonators on the soil's surface or embedded in the soil [1, 4]. Locally resonant seismic metasurfaces comprising an array of resonators are exploited in this paper.

In a uniform configuration, narrow band gaps around the resonance frequency of the resonators are provided [5]. Vibration mitigation in a wide frequency range is needed when the source is a broadband excitation, e.g. railway traffic [6]. Graded metamaterials have shown an attractive potential to broaden the band gap in homogeneous soils [7]. Depending on their arrangement, so-called metawedges can evoke rainbow trapping, which traps the Rayleigh wave and reflects the energy backward, or conversion of surface waves into shear waves propagating away from the surface of the homogeneous soil into the bulk.

The soil is actually a stratified medium, which in a good approximation is represented as a horizontally layered halfspace. As a result, body waves are partially reflected at layer interfaces,

propagating toward the surface of the soil. This hinders the surface-to-shear conversion evoked by inverse metawedges in a homogeneous medium [8]. Results considering 2D uniform and graded metasurfaces on layered soils were recently provided [9, 10]. 3D small-scale seismic metasurfaces and metabarriers on a heterogeneous medium were widely investigated [11, 12]. Results indicate that the soil profile has a significant impact on the vibration mitigation performance of seismic metamaterials, requiring further investigation.

This paper explores how the soil profile affects the vibration mitigation performance of seismic metasurfaces in a wide frequency band ($1 - 80\,\mathrm{Hz}$). The soil is represented as a horizontally layered medium. A uniform metasurface and a metawedge consisting of an array of graded resonators with increasing resonance frequency are considered. We assess the vibration mitigation performance of the metasurfaces by analyzing wavenumber-frequency spectra, transfer functions for a point load, and the wave field within the soil.

The outline of the paper is as follows. Section 2 presents a 3D FE-BE formulation for an array of resonators (metasurface) on layered soils. The vibration mitigation performance of uniform and graded seismic metasurfaces on homogeneous and layered soil is described in section 3. Section 4 concludes the paper.

2. 3D FE-BE formulation for multiple resonators on a layered halfspace

2.1. Problem outline

Figure 1 shows a metasurface composed of an array of N resonators on top of a layered soil represented by the unbounded domain $\Omega_{\mathrm{s}}^{\mathrm{e}}$. The first row of the metasurface is located at a perpendicular distance D from the origin of the coordinate system. The layout is characterized by a rectangular grid of N_x by N_y resonators with lattice constants a_x and a_y in the x- and y-direction, respectively. The interface between a resonator k and the soil is defined as Σ_k, while the soil-structure interface for N resonators is denoted as $\Sigma = \bigcup_{k=1}^{N} \Sigma_k$.

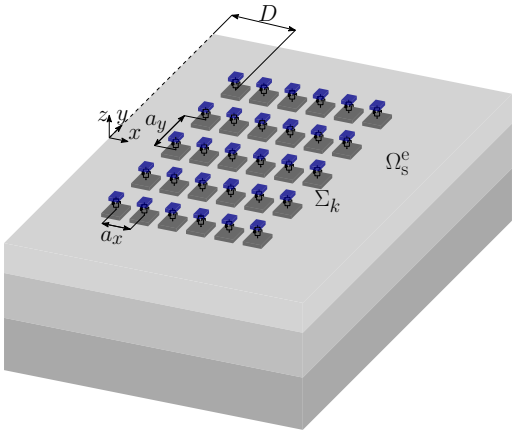

Figure 1: An array of resonators on top of a layered halfspace.

2.2. Displacement and traction fields

The displacement of a resonator k on top of the layered halfspace is denoted as $\hat{\mathbf{u}}_{\mathrm{r}k}(\mathbf{x}, \omega)$. A hat on a variable indicates its representation in the spatial-frequency domain. Continuity conditions and equilibrium of tractions are imposed on the soil-resonator interface Σ_k:

$$\hat{\mathbf{u}}_{\mathrm{r}k} - \hat{\mathbf{u}}_{\mathrm{s}} = \mathbf{0} \quad \text{on} \quad \Sigma_k \tag{1}$$

$$\hat{\mathbf{t}}_{\mathrm{r}}(\hat{\mathbf{u}}_{\mathrm{r}k}) + \hat{\mathbf{t}}_{\mathrm{s}}(\hat{\mathbf{u}}_{\mathrm{s}}) = \mathbf{0} \quad \text{on} \quad \Sigma_k, \tag{2}$$

where $\hat{\mathbf{u}}_\mathrm{s}(\mathbf{x},\omega)$ is the soil displacement vector and $\hat{\mathbf{t}}_\mathrm{r}(\hat{\mathbf{u}}_{\mathrm{r}k})(\mathbf{x},\omega)$ is the traction vector due to the displacement $\hat{\mathbf{u}}_{\mathrm{r}k}$.

Assuming that an incident wave field impinges on the resonators, the soil displacement $\hat{\mathbf{u}}_\mathrm{s}(\mathbf{x},\omega)$ is decomposed into the incident wave field $\hat{\mathbf{u}}_\mathrm{inc}(\mathbf{x},\omega)$, the locally diffracted wave field $\hat{\mathbf{u}}_\mathrm{d0}(\mathbf{x},\omega)$ and the wave field $\hat{\mathbf{u}}_\mathrm{sc}(\mathbf{x},\omega)$ scattered by displacements $\hat{\mathbf{u}}_{\mathrm{r}k}(\mathbf{x},\omega)$ of all resonators k ($k = 1,\ldots,N$) [13]:

$$\hat{\mathbf{u}}_\mathrm{s} = \hat{\mathbf{u}}_\mathrm{inc} + \hat{\mathbf{u}}_\mathrm{d0} + \sum_{k=1}^{N} \hat{\mathbf{u}}_\mathrm{sc}(\hat{\mathbf{u}}_{\mathrm{r}k}). \tag{3}$$

The incident wave field $\hat{\mathbf{u}}_\mathrm{inc}(\mathbf{x},\omega)$ is evaluated with a source model, the locally diffracted wave field $\hat{\mathbf{u}}_\mathrm{d0}(\mathbf{x},\omega)$ is an elastodynamic field that obeys the Sommerfeld's radiation condition. This is defined so that the combined wave field $\hat{\mathbf{u}}_\mathrm{inc}(\mathbf{x},\omega) + \hat{\mathbf{u}}_\mathrm{d0}(\mathbf{x},\omega)$ vanishes on the soil-structure interface Σ.

2.3. The dynamic soil-structure interaction problem

The dynamic equilibrium for a single structure j ($j = 1,\ldots,N$) can be expressed in a weak variational form. A virtual displacement field $\hat{\mathbf{v}}_{\mathrm{r}j}(\mathbf{x},\omega)$ is imposed on the structure j in order to construct the virtual work expression for the dynamic soil-structure interaction problem [14]:

$$\begin{aligned}\int_{\Omega_{\mathrm{r}j}} \hat{\boldsymbol{\epsilon}}_\mathrm{r}(\hat{\mathbf{v}}_{\mathrm{r}j}) : \hat{\boldsymbol{\sigma}}_\mathrm{r}(\hat{\mathbf{u}}_{\mathrm{r}j})\,\mathrm{d}\Omega - \omega^2 \int_{\Omega_{\mathrm{r}j}} \hat{\mathbf{v}}_{\mathrm{r}j}\cdot\rho_{\mathrm{r}j}\hat{\mathbf{u}}_{\mathrm{r}j}\,\mathrm{d}\Omega + \sum_{k=1}^{N}\int_{\Sigma_j} \hat{\mathbf{v}}_{\mathrm{r}j}\cdot\hat{\mathbf{t}}_\mathrm{s}(\hat{\mathbf{u}}_\mathrm{sc}(\hat{\mathbf{u}}_{\mathrm{r}k}))\,\mathrm{d}\Gamma \\ = -\int_{\Sigma_j} \hat{\mathbf{v}}_{\mathrm{r}j}\cdot\hat{\mathbf{t}}_\mathrm{s}(\hat{\mathbf{u}}_\mathrm{inc}+\hat{\mathbf{u}}_\mathrm{d0})\,\mathrm{d}\Gamma.\end{aligned} \tag{4}$$

where $\hat{\boldsymbol{\epsilon}}_\mathrm{r}(\hat{\mathbf{v}}_{\mathrm{r}j})(\mathbf{x},\omega)$ is the virtual strain tensor, $\hat{\boldsymbol{\sigma}}_\mathrm{r}(\hat{\mathbf{u}}_{\mathrm{r}j})(\mathbf{x},\omega)$ is the Cauchy stress tensor due to displacements $\hat{\mathbf{u}}_{\mathrm{r}j}(\mathbf{x},\omega)$, and $\rho_{\mathrm{r}j}$ is the density of the structure.

This problem is solved by means of a coupled FE-BE model. The resonator is modeled with finite elements whereas boundary elements are used to discretize the unbounded soil on the interfaces Σ_k. The structural displacement vector for resonator j is discretized as:

$$\hat{\mathbf{u}}_{\mathrm{r}j} \simeq \mathbf{N}_{\mathrm{r}j}\underline{\hat{\mathbf{u}}}_{\mathrm{r}j}, \tag{5}$$

where $\mathbf{N}_{\mathrm{r}j}$ is a matrix of global finite element shape functions for resonator j and $\underline{\hat{\mathbf{u}}}_{\mathrm{r}j}(\omega)$ is the vector with nodal degrees of freedom. In a Galerkin approach, this approximation is also used for the virtual displacement field $\hat{\mathbf{v}}_\mathrm{r}(\mathbf{x},\omega)$. Equation (4) then yields:

$$\left[\mathbf{K}_j - \omega^2\mathbf{M}_j\right]\underline{\hat{\mathbf{u}}}_{\mathrm{r}j} + \sum_{k=1}^{N}\hat{\mathbf{K}}^\mathrm{s}_{jk}\underline{\hat{\mathbf{u}}}_{\mathrm{r}k} = \underline{\hat{\mathbf{f}}}^\mathrm{s}_j, \tag{6}$$

where $\mathbf{K}_j$ and $\mathbf{M}_j$ are the stiffness and mass matrices of the resonator j, respectively. The contribution of structural damping can be added to equation (6). In this work, proportional damping is used where a damping ratio is defined for each mode of the structure. The summation in equation (6) accounts for through-soil coupling of resonator j with all resonators. The soil stiffness matrix $\hat{\mathbf{K}}^\mathrm{s}_{jk}(\omega)$ is given by:

$$\hat{\mathbf{K}}^\mathrm{s}_{jk} = \int_{\Sigma_j} \mathbf{N}^\mathrm{T}_{\mathrm{r}j}\hat{\mathbf{t}}_\mathrm{s}(\hat{\mathbf{u}}_\mathrm{sc}(\mathbf{N}_{\mathrm{r}k}))\,\mathrm{d}\Gamma. \tag{7}$$

The force vector $\hat{\underline{\mathbf{f}}}^{\mathrm{s}}_j(\omega)$ due to an incident wave field is equal to:

$$\hat{\underline{\mathbf{f}}}^{\mathrm{s}}_j = -\int_{\Sigma_j} \mathbf{N}^{\mathrm{T}}_{\mathrm{r}j}\hat{\mathbf{t}}_{\mathrm{s}}(\hat{\mathbf{u}}_{\mathrm{inc}} + \hat{\mathbf{u}}_{\mathrm{d0}})\,\mathrm{d}\Gamma. \tag{8}$$

The scattered wave field and the locally diffracted wave field are computed by means of the BE method, as the problem is formulated in terms of displacements on the interfaces Σ_k. When the resonator j is placed on the surface of the soil, $\hat{\mathbf{t}}_{\mathrm{s}}(\hat{\mathbf{u}}_{\mathrm{inc}})(\omega) = \mathbf{0}$. The tractions $\hat{\mathbf{t}}_{\mathrm{s}k}(\omega)$ on the soil-resonator interfaces Σ_k are calculated as:

$$\sum_{k=1}^{N}\left[\mathbf{I}_{jk} + \hat{\mathbf{T}}_{jk}\right]\hat{\underline{\mathbf{u}}}_{\mathrm{s}k} = \sum_{k=1}^{N}\hat{\mathbf{U}}_{jk}\hat{\underline{\mathbf{t}}}_{\mathrm{s}k}, \tag{9}$$

where $\mathbf{I}_{jk}$ is an identity matrix, $\hat{\mathbf{U}}_{jk}(\omega)$ and $\hat{\mathbf{T}}_{jk}(\omega)$ are fully populated asymmetric boundary element matrices which require the integration of Green's functions for a layered halfspace, and $\hat{\underline{\mathbf{u}}}_{\mathrm{s}k}(\omega)$ and $\hat{\underline{\mathbf{t}}}_{\mathrm{s}k}(\omega)$ are the displacements and tractions on the soil-structure interface Σ_k. For a BE mesh on the surface of the soil, $\hat{\mathbf{T}}_{jk}(\omega) = \mathbf{0}$.

2.4. Craig-Bampton substructuring technique

The resonator comprises a superstructure coupled to a foundation resting on the surface of the soil. Therefore, it is convenient to decompose the displacement vector $\hat{\underline{\mathbf{u}}}_{\mathrm{r}j}$ of resonator j into displacements of its foundation $\hat{\underline{\mathbf{u}}}_{\mathrm{r}_1 j}$ and superstructure $\hat{\underline{\mathbf{u}}}_{\mathrm{r}_2 j}$. The use of a Craig-Bampton substructuring technique reduces the problem size and avoids the recomputation of the BE matrices for alternative superstructures [15]. Using the Craig-Bampton substructuring technique, the structural displacement vector for resonator j is discretized as:

$$\hat{\mathbf{u}}_{\mathrm{r}j} \simeq \begin{bmatrix} \mathbf{N}_{\mathrm{r}_1 j} & \mathbf{N}_{\mathrm{r}_2 j} \end{bmatrix}\begin{bmatrix} \boldsymbol{\Phi}_{\mathrm{r}_1 j} & \mathbf{0} \\ \boldsymbol{\Phi}^{\mathrm{s}}_{\mathrm{r}_2 j} & \boldsymbol{\Phi}_{\mathrm{r}_2 j} \end{bmatrix}\begin{Bmatrix} \hat{\underline{\boldsymbol{\alpha}}}_{\mathrm{r}_1 j} \\ \hat{\underline{\boldsymbol{\alpha}}}_{\mathrm{r}_2 j} \end{Bmatrix} = \mathbf{N}_{\mathrm{r}j}\boldsymbol{\Phi}_{\mathrm{r}j}\hat{\underline{\boldsymbol{\alpha}}}_{\mathrm{r}j}, \tag{10}$$

where the vector $\hat{\underline{\boldsymbol{\alpha}}}_{\mathrm{r}j}(\omega)$ collects the modal coordinates. The modes $\boldsymbol{\Phi}_{\mathrm{r}_2 j}$ are the eigenmodes of the superstructure with clamped base. The modes $\boldsymbol{\Phi}_{\mathrm{r}_1 j}$ are the eigenmodes of the foundation without the superstructure. The modes $\boldsymbol{\Phi}^{\mathrm{s}}_{\mathrm{r}_2 j}$ are the quasi-static transmission of the foundation modes $\boldsymbol{\Phi}_{\mathrm{r}_1 j}$ into the superstructure:

$$\boldsymbol{\Phi}^{\mathrm{s}}_{\mathrm{r}_2 j} = -\mathbf{K}^{-1}_{\mathrm{r}_2\mathrm{r}_2 j}\mathbf{K}_{\mathrm{r}_2\mathrm{r}_1 j}\boldsymbol{\Phi}_{\mathrm{r}_1 j}, \tag{11}$$

where $\mathbf{K}_{\mathrm{r}_2\mathrm{r}_2 j}$ and $\mathbf{K}_{\mathrm{r}_2\mathrm{r}_1 j}$ are submatrices of the stiffness matrix of the resonator j defined according to the degrees of freedom of the foundation r_2 and superstructure r_1. Using a Galerkin approach, substituting equation (10) into equation (4), and premultiplying with $\boldsymbol{\Phi}^{\mathrm{T}}_{\mathrm{r}j}$ yields:

$$\boldsymbol{\Phi}^{\mathrm{T}}_{\mathrm{r}j}\left[\mathbf{K}_j - \omega^2\mathbf{M}_j\right]\boldsymbol{\Phi}_{\mathrm{r}j}\hat{\underline{\boldsymbol{\alpha}}}_{\mathrm{r}j} + \sum_{k=1}^{N}\boldsymbol{\Phi}^{\mathrm{T}}_{\mathrm{r}j}\hat{\mathbf{K}}^{\mathrm{s}}_{jk}\boldsymbol{\Phi}_{\mathrm{r}k}\hat{\underline{\boldsymbol{\alpha}}}_{\mathrm{r}k} = \boldsymbol{\Phi}^{\mathrm{T}}_{\mathrm{r}j}\hat{\underline{\mathbf{f}}}^{\mathrm{s}}_j. \tag{12}$$

The modal soil stiffness matrix $\boldsymbol{\Phi}^{\mathrm{T}}_{\mathrm{r}j}\hat{\mathbf{K}}^{\mathrm{s}}_{jk}\boldsymbol{\Phi}_{\mathrm{r}k}$ is given by:

$$\boldsymbol{\Phi}^{\mathrm{T}}_{\mathrm{r}j}\hat{\mathbf{K}}^{\mathrm{s}}_{jk}\boldsymbol{\Phi}_{\mathrm{r}k} = \int_{\Sigma_j}\boldsymbol{\Phi}^{\mathrm{T}}_{\mathrm{r}j}\mathbf{N}^{\mathrm{T}}_{\mathrm{r}j}\hat{\mathbf{t}}_{\mathrm{s}}(\hat{\mathbf{u}}_{\mathrm{sc}}(\mathbf{N}_{\mathrm{r}k}\boldsymbol{\Phi}_{\mathrm{r}k}))\,\mathrm{d}\Gamma. \tag{13}$$

The modal soil tractions $\hat{\mathbf{t}}_{\mathrm{s}}(\hat{\mathbf{u}}_{\mathrm{sc}}(\mathbf{N}_{\mathrm{r}_1 k}\boldsymbol{\Phi}_{\mathrm{r}_1 k}))$ are computed by means of equation (9) for each mode and integrated over the interface using equation (13). Any change of the superstructure does not affect the computation of the soil stiffness (13) as this term only depends on the BE mesh.

2.5. Receiver points

Tractions $\hat{\underline{\mathbf{t}}}_{\mathrm{s}}(\omega)$ and displacements $\hat{\underline{\mathbf{u}}}_{\mathrm{s}}(\omega)$ on the soil-resonators interface Σ are computed according to [5]. The radiated wave field $\hat{\underline{\mathbf{u}}}^{\mathrm{r}}_{\mathrm{s}}(\mathbf{x},\omega)$ within the soil domain can be evaluated as:

$$\hat{\underline{\mathbf{u}}}^{\mathrm{r}}_{\mathrm{s}} = \hat{\mathbf{U}}_{\mathrm{p}}\hat{\underline{\mathbf{t}}}_{\mathrm{s}} - \hat{\mathbf{T}}_{\mathrm{p}}\hat{\underline{\mathbf{u}}}_{\mathrm{s}}, \tag{14}$$

where $\hat{\mathbf{U}}_{\mathrm{p}}(\mathbf{x},\omega)$ and $\hat{\mathbf{T}}_{\mathrm{p}}(\mathbf{x},\omega)$ are boundary element transfer matrices computed based on the Green's functions of a layered halfspace.

3. Vibration reduction by seismic metasurfaces

3.1. Problem outline

A 2D array of $N_x = 12$ by $N_y = 10$ resonators on top of homogeneous and layered soil is considered. The dynamic soil characteristics are summarized in tables 1 and 2. The layered soil (table 2) is composed of a single layer on top of a halfspace four times stiffer than the layer. The layer has the same properties of the homogeneous halfspace described in table 1. The layer thickness h is chosen such that the cut-on frequency of the soil ($\approx 15\,\mathrm{Hz}$) falls below the resonance frequencies of the resonators.

The resonator is composed of an oscillator attached to a surface foundation. For the uniform metasurface, the oscillator has a mass of 50 kg and a resonance frequency of 60 Hz ($j = 1, \ldots, N$). For the graded metasurfaces, the stiffness of the oscillators is graded conserving the mass, yielding a linear variation of the resonators' eigenfrequencies in the x-direction. A damping ratio $\xi = 0.01$ is assumed for both cases. The foundation is modeled as a rigid concrete slab with $L^{\mathrm{f}}_x = L^{\mathrm{f}}_y = 0.5\,\mathrm{m}$, thickness 0.1 m and mass 62.5 kg. The seismic metasurface is placed far from the source, $D = 30\,\mathrm{m}$, in order to study its vibration mitigation performance when excited by Rayleigh waves generated by a harmonic point load.

Layer	h [m]	C_{s} [m/s]	C_{p} [m/s]	β_{s} [-]	β_{p} [-]	ρ [kg/m^3]
1	∞	150	300	0.020	0.020	1800

Table 1: Dynamic soil characteristics for the homogeneous soil.

Layer	h [m]	C_{s} [m/s]	C_{p} [m/s]	β_{s} [-]	β_{p} [-]	ρ [kg/m^3]
1	5	150	300	0.020	0.020	1800
2	∞	300	600	0.020	0.020	1800

Table 2: Dynamic soil characteristics for the layered soil.

3.2. Algorithmic parameters

The vertical mobility $\hat{v}_{zz}(x, y = 0, z = 0, \omega)$ is computed on a wide range of receiver points in the x-direction. Computations are made for frequencies between 1 and 80 Hz with a frequency bin of 1 Hz. A logarithmic sampling is adopted for the spatial coordinate x and the horizontal wavenumber k_x. The wavenumber-frequency spectra $\tilde{v}_{zz}(k_x, y = 0, z = 0, \omega)$ are assessed by means of a forward Fourier transform from the horizontal coordinate x to the horizontal wavenumber k_x.

3.3. Homogeneous soil

3.3.1. Uniform metasurface The results in this subsection were originally presented by Carneiro et al. [5]. They are summarized here to allow the comparison of two different soil profiles.

A uniform metasurface (figure 2a) on the homogeneous soil creates a narrow band gap around the resonance frequency of the oscillators (figure 2b). The wavenumber-frequency spectrum computed using the 3D FE-BE model agrees with the analytical dispersion curve of an infinite number of resonators interacting with the homogeneous halfspace [4]. Figure 2c shows the vertical soil mobility $\hat{v}_{zz}(x = 57.35\,\mathrm{m}, y = 0, z = 0, \omega)$ on a logarithmic scale in dB with a reference mobility of $10^{-8}\,\mathrm{m/s/N}$. The free field response is used as the reference case. At these frequencies, a large vibration mitigation is found behind the metasurface (figure 2c). The real part of the vertical displacement is computed on a large grid of receiver points (figures 2d-f). The resonators are depicted by black squares on the surface of the soil. The vibration mitigation mechanism consists of a Rayleigh wave converted into a shear wave propagating from the surface into the bulk (figure 2e). The Rayleigh wave still propagates behind the array of resonators, but its amplitude is lower than the free field response. The waves are not affected by the metasurfaces at frequencies far from the resonance frequency of the resonators (figures 2d and 2f).

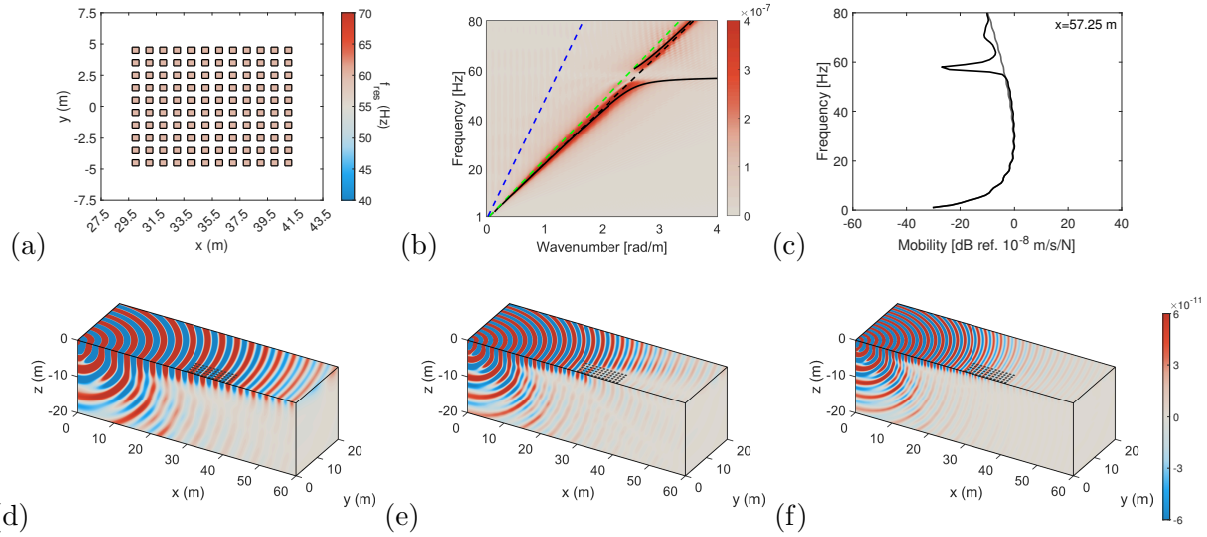

Figure 2: (a) Eigenfrequencies for a uniform array of $N_x = 12$ by $N_y = 10$ resonators. (b) Modulus of the vertical mobility $\tilde{v}_{zz}(k_x, y = 0, z = 0, \omega)$. Superimposed are the dispersion curves of the dilatational (■), shear (■), and Rayleigh (■) wave propagating in the free halfspace and the analytical dispersion curve of an infinite number of resonators interacting with a homogeneous halfspace (solid line). (c) The vertical soil mobility $\hat{v}_{zz}(x = 57.25\,\mathrm{m}, y = 0, z = 0, \omega)$ without and with resonators. Real part of the vertical displacement $\hat{u}_{zz}(\mathbf{x}, \mathbf{x}', \omega)$ [m/Hz] at (d) 40 Hz, (e) 60 Hz, and (f) 80 Hz.

3.3.2. Graded metasurface The band gap created by a uniform array of resonators can be widened by considering graded metasurfaces. This is accomplished by tuning the properties of the oscillators so that their resonance frequency is smoothly graded in the x-direction. These are so-called metawedges, first presented by Colombi et al. [7]. In this paper, only the performance of inverse metawedges, i.e., resonators with increasing eigenfrequency, will be investigated.

Since only the superstructure is modified and a Craig-Bampton substructuring method is applied, the recomputation of the soil stiffness matrix and the boundary element transfer

matrices is avoided. The computational time is therefore drastically reduced.

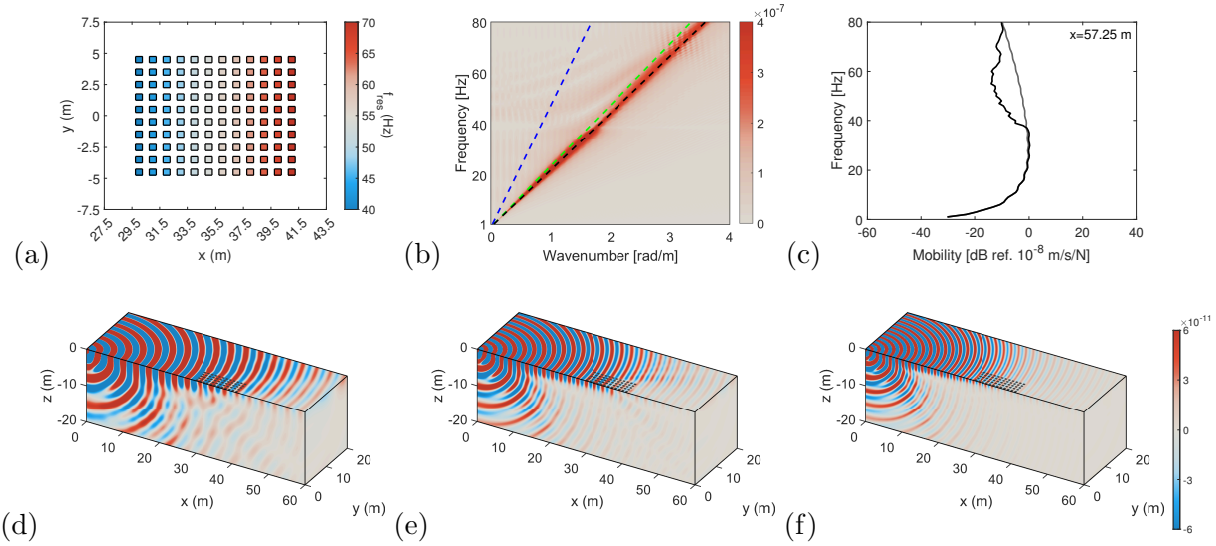

Figure 3: (a) Eigenfrequencies for a graded array of $N_x = 12$ by $N_y = 10$ resonators. (b) Modulus of the vertical mobility $\tilde{v}_{zz}(k_x, y = 0, z = 0, \omega)$. Superimposed are the dispersion curves of the dilatational (■), shear (■), and Rayleigh (■) wave propagating in the free halfspace. (c) The vertical soil mobility $\hat{v}_{zz}(x = 57.25\,\mathrm{m}, y = 0, z = 0, \omega)$ without and with resonators. Real part of the vertical displacement $\hat{u}_{zz}(\mathbf{x}, \mathbf{x}', \omega)$ [m/Hz] at (d) 40 Hz, (e) 60 Hz, and (f) 80 Hz.

The graded metasurface is built changing the stiffness while the mass of the oscillator is maintained constant. Figure 3a shows the resonance frequencies of the considered inverse metawedge, ranging from 40 Hz to 70 Hz. The peak values of the wavenumber-frequency spectrum are reduced within this range (figure 3b). The mobility is substantially reduced between 40 Hz and 70 Hz (figure 3c).

The real part of the vertical displacement at 40 Hz, 60 Hz, and 80 Hz is shown in figures 3d-f. When the wavefront reaches the row of resonators of eigenfrequency equal to the excitation frequency, a conversion of Rayleigh waves into shear waves propagating into the bulk is observed. Attenuated Rayleigh waves still propagate behind the metasurface, as a consequence of the finite number of resonators in the x-direction. At 80 Hz, the Rayleigh wave is not affected by the resonators, as the maximum resonance frequency of the metasurface is 70 Hz.

3.4. Layered soil

In this section, the uniform metasurface and the inverse metawedge used in section 3.3 are placed on top of the layered soil described in table 2.

3.4.1. Uniform metasurface Figure 4b shows the wavenumber-frequency spectrum for a uniform array of $N_x = 12$ by $N_y = 10$ resonators, presented in figure 4a, on top of the layered halfspace. Superimposed are the dispersion curves of the first six Rayleigh wave modes of the layered halfspace without resonators. The wavenumber-frequency response is mostly governed by the fundamental Rayleigh wave mode as the maxima of the spectrum follow the first mode. At low wavenumber values, body waves are characterized by dips and peaks in the response, but their amplitude is much lower than the fundamental mode. A peak is observed at the cut-on frequency of 15 Hz.

Mainly the fundamental mode is affected by the metasurface around 60 Hz, resulting in a partial band gap in the wavenumber-frequency response. The analytical dispersion curve

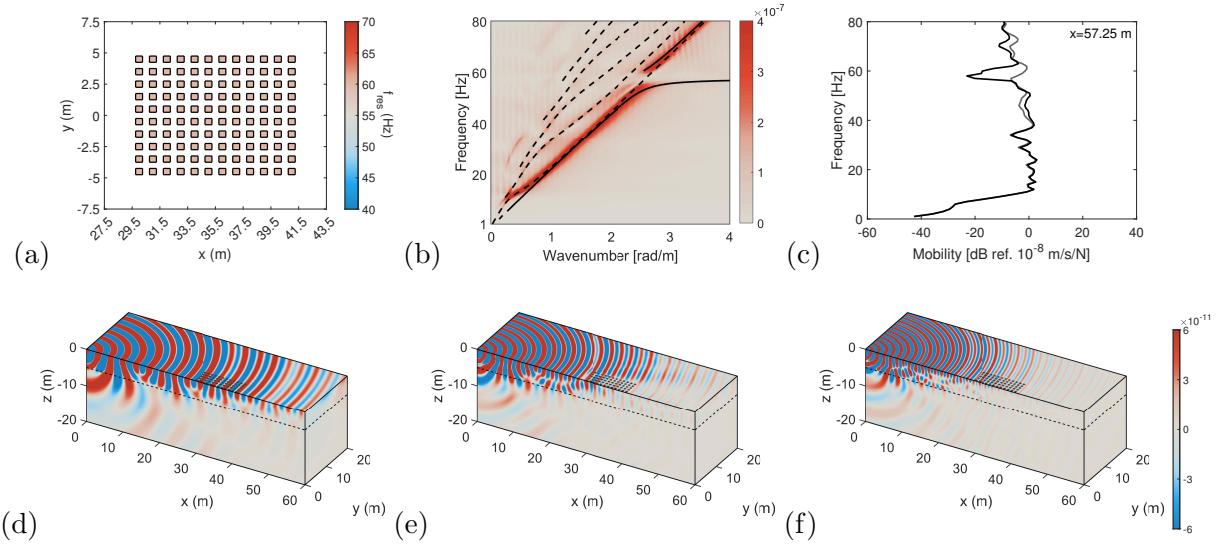

Figure 4: (a) Eigenfrequencies for a uniform array of $N_x = 12$ by $N_y = 10$ resonators. (b) Modulus of the vertical mobility $\tilde{v}_{zz}(k_x, y = 0, z = 0, \omega)$. Superimposed are the dispersion curves of the first six Rayleigh wave modes (dashed lines) and the analytical dispersion curve of an infinite number of resonators interacting with a homogeneous halfspace (solid line). (c) The vertical soil mobility $\hat{v}_{zz}(x = 57.25\,\text{m}, y = 0, z = 0, \omega)$ without and with resonators. Real part of the vertical displacement $\hat{u}_{zz}(\mathbf{x}, \mathbf{x}', \omega)$ [m/Hz] at (d) 40 Hz, (e) 60 Hz, and (f) 80 Hz. The dashed lines indicate the layer interface.

presented in figure 2b is also superimposed in figure 4b. A good agreement between the opening on the fundamental mode of the layered soil and the analytical dispersion curve is observed. However, this only holds for layered soils of cut-on frequency below the oscillators' resonance frequency.

Large vibration reduction is found in the mobility response (figure 4c) at frequencies corresponding to the opening in the fundamental mode. A slight frequency shift in the response is observed between the mobility without and with the array of resonators. Surface masses modify the mass density of the system, resulting in a change in the Rayleigh wave velocity, and shifting frequency [16].

Figures 4d-f show the wave propagation within the layered soil with metasurface at 40 Hz, 60 Hz, and 80 Hz, respectively. Several constructive and destructive interferences characterize the complex wave propagation in layered soil. Waves are faster and have longer wavelengths in the stiffer halfspace than in the layer. No prominent attenuation effect is noticed in figures 4d and 4f, agreeing with the mobility response in figure 4c. The surface-to-shear conversion observed in the homogeneous halfspace (figure 2e) is not seen in layered soil (figure 4e). The array of resonators is triggered by the wave propagation at the surface of the soil yielding the hybridization effect. At 60 Hz, a surface-to-bulk mode conversion is expected as the Rayleigh wave still bends towards the shear wave in figure 4b. The transformed waves are, however, mainly trapped within the layer (figure 4e). Large vibration mitigation is still observed behind the metasurface, which is non-uniform due to wave reflections within the layer, in contrast to the uniform attenuation observed in figure 2. The mobility response is significantly distinct at different receiver points behind the metasurface.

3.4.2. Graded metasurface The inverse metawedge presented in figure 5a is placed on top of the layered halfspace. Figures 5b and 5c show the effect of the metawedge on the wavenumber-

frequency spectrum and the mobility response, respectively. Although the metawedge produces lower vibration reduction in comparison to the case of uniform metasurface, vibration mitigation in a broad frequency band (40 Hz - 70 Hz) is still evoked using metawedges in layered soil. The efficiency of the metawedge is mostly reduced when the results in homogeneous (figure 3c) and layered (figure 5c) soils are compared.

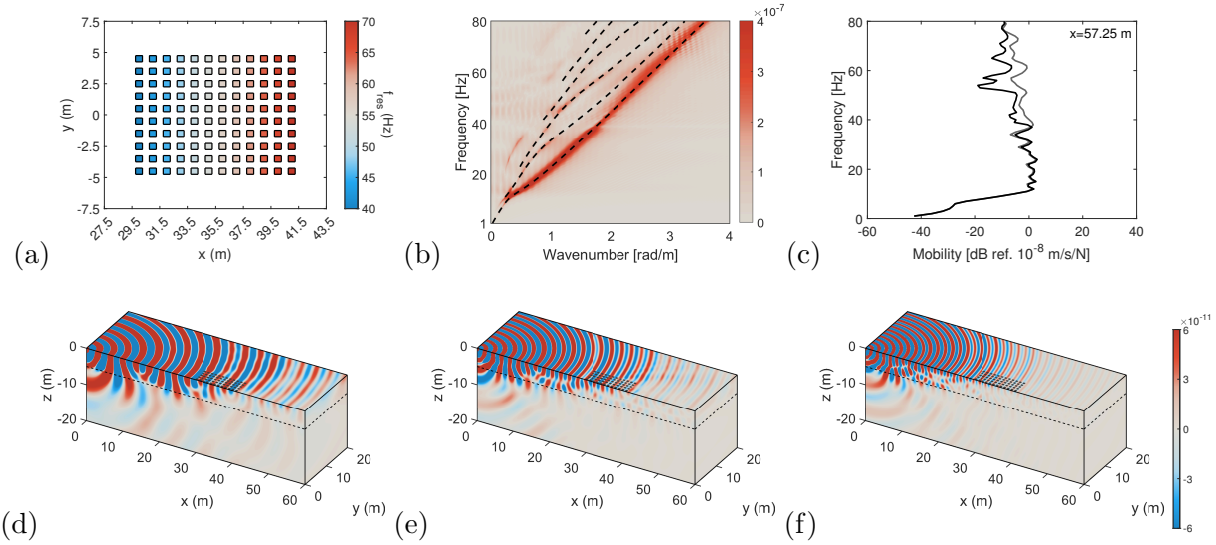

Figure 5: (a) Eigenfrequencies for a graded array of $N_x = 12$ by $N_y = 10$ resonators. (b) Modulus of the vertical mobility $\tilde{v}_{zz}(k_x, y = 0, z = 0, \omega)$. Superimposed are the dispersion curves of the first six Rayleigh wave modes (dashed lines). (c) The vertical soil mobility $\hat{v}_{zz}(x = 57.25\,\mathrm{m}, y = 0, z = 0, \omega)$ without and with resonators. Real part of the vertical displacement $\hat{u}_{zz}(\mathbf{x}, \mathbf{x}', \omega)$ [m/Hz] at (d) 40 Hz, (e) 60 Hz, and (f) 80 Hz. The dashed lines indicate the layer interface.

The wave field in the layered soil with the inverse metawedge at 40 Hz, 60 Hz, and 80 Hz is shown in figures 5d-f. The metasurface is still activated when the wavefront reaches the row of resonators of resonance frequency equal to the excitation frequency and, hence, vibration reduction is obtained from this point onwards at the surface of the soil. A comparison between figures 4d and 5d shows that body waves with long wavelength propagating in the halfspace from $x = 40$ m onwards are observed at 40 Hz. This indicates that the surface-to-shear wave conversion induced by inverse metawedges in homogeneous media (figures 3d and 3e) still arises, even though the shear wave is predominantly trapped within the layer. At 60 Hz, this effect is less noticeable. Nevertheless, considerable vibration mitigation is observed behind the metasurface at the surface of the soil. Again, the graded metasurface is not activated at 80 Hz as the maximum resonance frequency is 70 Hz.

4. Conclusions

This paper investigates how the dynamic soil characteristics affect the vibration attenuation performance of seismic metasurfaces in a wide frequency band. A 3D FE-BE model using Craig-Bampton substructuring method is implemented to perform the analyses. Uniform and graded metasurfaces on homogeneous and layered soil are considered. The layered soil has a cut-on frequency below the resonance frequency of the oscillators. A uniform metasurface on the homogeneous soil creates a narrow band gap for all wavenumbers, whereas it mainly affects the fundamental mode of a layered soil. Significant vibration reduction is obtained at these

frequencies. The inverse metawedge evokes vibration attenuation in a broad frequency band in both homogeneous and layered soil. In the latter, however, their efficiency is reduced. The attenuation mechanism is the same, but the converted body waves are trapped within the layer. Graded metasurfaces can be tuned to attenuate a wide frequency content of railway induced vibration in homogeneous or layered soils.

Acknowledgement
Results presented in this paper were obtained within the frame of the project G0B8221N "Mitigation of railway induced vibration using seismic metamaterials" funded by the Research Foundation Flanders (FWO Flanders). The financial support is gratefully acknowledged.

References

[1] Colquitt D, Colombi A, Craster R, Roux P and Guenneau S 2017 *Journal of the Mechanics and Physics of Solids* **99** 379–393
[2] Brûlé S, Javelaud E, Enoch S and Guenneau S 2014 *Physical Review Letters* **112** 133901
[3] Wagner P, Dertimanis V, Antoniadis I and Chatzi E 2016 *International Journal of Earthquake and Impact Engineering* **1** 20–56
[4] Palermo A, Krödel S, Marzani A and Daraio C 2016 *Scientific Reports* **6** 1–10
[5] Carneiro D, Kato H, Reumers P, Lombaert G and Degrande G 2022 Mitigation of environmental ground vibration using seismic metasurfaces *Proceedings of the 30th International Conference on Noise and Vibration Engineering, ISMA 2022* ed Desmet W, Pluymers B, Moens D and Neeckx S (Leuven, Belgium) pp 3247–3261
[6] Lombaert G and Degrande G 2009 *Journal of Sound and Vibration* **319** 1036–1066 URL `http://dx.doi.org/10.1016/j.jsv.2008.07.003`
[7] Colombi A, Colquitt D, Roux P, Guenneau S and Craster R 2016 *Scientific reports* **6** 1–6
[8] Zeng C, Zhao C and Zeighami F 2022 *Earthquake Engineering and Structural Dynamics* **51** 1201–1223
[9] Zeighami F, Palermo A, Vratsikidis A, Cheng Z, Pitilakis D and Marzani A 2021 *Mechanics Based Design of Structures and Machines* **49** 1157–1172
[10] He C, Zhou S, Li X, Di H and Zhang X 2023 *Construction and Building Materials* **363** 129769
[11] Zaccherini R, Colombi A, Palermo A, Dertimanis V, Marzani A, Thomsen H, Stojadinovic B and Chatzi E 2020 *Physical Review Applied* **13** 034055
[12] Zaccherini R, Palermo A, Marzani A, Colombi A, Dertimanis V and Chatzi E 2020 *Applied Physics Letters* **117** 254103
[13] Aubry D and Clouteau D 1992 A subdomain approach to dynamic soil-structure interaction *Recent advances in Earthquake Engineering and Structural Dynamics* ed Davidovici V and Clough R (Nantes: Ouest Editions/AFPS) pp 251–272
[14] François S, Schevenels M, Lombaert G, Galvín P and Degrande G 2010 *Computer Methods in Applied Mechanics and Engineering* **199** 1536–1548 URL `http://dx.doi.org/10.1016/j.cma.2010.01.001`
[15] Craig R and Bampton M 1968 *AIAA Journal* **6** 1313–1319
[16] Schevenels M, Degrande G and Lombaert G 2004 *International Journal for Numerical and Analytical Methods in Geomechanics* **28** 395–419 URL `http://dx.doi.org/10.1002/nag.342`